JMEPEG (2012) 21:143–152
DOI: 10.1007/s11665-011-9896-1

1059-9495/$19.00

Simulation of Aluminum Powder in Tube Compaction Using Equal Channel Angular Extrusion

Reza Derakhshandeh Haghighi, Ahmad Jenabali Jahromi, and Behnam Esfandiar Jahromi

(Submitted November 4, 2010; in revised form February 9, 2011)

Aluminum powder in tube compaction with a 25 mm front plug through equal channel angular extrusion (ECAE) at room temperature was modeled using the finite element analysis package ABAQUS. The Gurson model was used in modeling this process. 2-D simulations in a 90° angle die showed better consolidation of powder near the inner edge of the die than the outer edge after one pass of ECAE but almost full densification occurs after two passes. The effect of hydrostatic pressure on densification of the powder was investigated by using two plugs varying in length dimension. The results obtained from the simulations were also compared with experiments conducted to compact aluminum powder with mean particle diameter of 45 μm. Optical microscopy, microhardness test, and density measurements confirmed the simulations. The simulations were extended to powder compaction in a 60° and 120° angle die. It was found that one pass of ECAE is sufficient to consolidate the aluminum powder completely and uniformly in a 60° angle die, whereas the material is still porous in a 120° angle die.

Keywords equal channel angular extrusion, finite element modeling, hydrostatic pressure, powder compaction

1. Introduction

In recent years, equal channel angular extrusion (ECAE) has been used as a method to produce ultra fine-grained materials (Ref 1-4). It is an effective method to produce a large amount of simple shear deformation in a material by pressing it around a corner of two intersecting channels with equal cross sections (Ref 5, 6). The main advantage of ECAE over conventional extrusion is that the cross section of the material remains the same after the process and thus it can be passed through the same die to repeat the process and in fact higher plastic deformation is accumulated (Ref 7). In addition, the deformation is quite uniform as compared to conventional deformation processes and also the low load requirements for processing. Many studies have been conducted to model the ECAE process for solid billets. In most of them, the effect of processing parameters such as die shape and friction and analyzing the plastic deformation behavior of the process have been investigated (Ref 8-21).

Recently, ECAE has also been used for compaction of powders, mainly by putting the powder in a can or tube and passing it through an ECAE die or by applying back pressure (Ref 22-25). The main goals of these works were to achieve full densification of powders and to enhance the mechanical property of the compacts. Moreover, powder compaction by ECAE is better done at lower temperatures than hot isostatic pressing (HIP), which is an expensive and relatively time-consuming process. Single pass and multiple pass ECAE has been used to compact a wide variety of powders such as pure metallic elemental (Ref 25), alloys (Ref 26), and amorphous (Ref 27) powders to near the theoretical densities.

Most of the researches have been done on simulation of simple compaction or multiaxial compaction of powders (Ref 28-30), and some have been conducted on powder consolidation via ECAE, for example, Kim et al. worked on equal channel angular pressing of metallic powders (Ref 31) to achieve both powder consolidation and grain refinement. Yoon et al. (Ref 32) investigated the consolidation, plastic deformation, and microstructure evolution behavior of Al-Si powders during ECAP using experimental and theoretical methods. Almost independent behavior of powder densification in the entry channel and shear deformation in the main deformation zone was found by the finite element method in conjunction with a pressure-dependent material yield model. It was found that high mechanical strength could be achieved effectively as a result of the well-bonded powder contact surface during ECAP process of gas atomized Al-Si powders. Yoon et al. (Ref 33) also investigated the mechanical properties of hypereutectic Al-20 wt.% Si alloy up to eight passes of ECAE and it was found that ECAE is effective in matrix grain and Si particle refinement. Finite element analysis for deformation behavior of an aluminum alloy composite containing SiC particles and porosities during ECAE has been carried out by Lee et al. (Ref 34). They showed that the powder reaches near full density before it enters the corner, but no tube or back pressure was applied. Without a tube these simulations do not represent actual powder compaction, because the tube has a substantial effect on the amount of hydrostatic pressure.

In this study, efforts were duly made in the modeling of densification of aluminum powder in tube through multipass ECAE at room temperature using Gurson model (Ref 35), which is an effective model for high density porous materials

Reza Derakhshandeh Haghighi and **Ahmad Jenabali Jahromi**, Department of Materials Science and Engineering, School of Engineering, Shiraz University, Shiraz, Iran; and **Behnam Esfandiar Jahromi**, Department of Mechanical Engineering, Politecnico di Milano University, Milan, Italy. Contact e-mails: jahromi@shirazu.ac.ir and derakhshande@shirazu.ac.ir.

and also the effect of hydrostatic pressure on densification of the powder was investigated by using two plugs varying in length dimension and the simulations were extended to 60° and 120° angle die. Finite element analysis was carried out using ABAQUS/Explicit (Ref 36), and then the simulations were evaluated with experimental results.

2. Modeling

Many models and consolidation mechanisms have been proposed to simulate powder compaction (Ref 35, 37, 38). Different plastic yield functions such as Shima-Oyane, Green, Gurson, etc., have been developed for porous materials until now which satisfy the required conditions. In this article, the Gurson model was used due to capability of the ABAQUS software for modeling this yield function model and also the effectiveness of this model for high density porous materials. From plastic response of a hollow sphere model, Gurson proposed the yield function for a porous material which is useful in the high density region with a relative density >0.9. Thus,

$$\Phi = \left(\frac{q}{\sigma_y}\right)^2 + 2f\cosh\left(\frac{-3P}{2\sigma_y}\right) - (1+f^2), \qquad \text{(Eq 1)}$$

where $P = -\frac{1}{3}\boldsymbol{\sigma} : 1$ is the hydrostatic pressure, $S = PI + \boldsymbol{\sigma}$ is the deviatoric part of the Cauchy stress tensor $\boldsymbol{\sigma}$, $q = \sqrt{(3/2)S : S}$ is the effective Mises stress, f is the void volume fraction (porosity), and σ_y is the yield stress of the fully dense matrix material. The Gurson model accounted for plastic dilatancy which is characteristic to porous ductile materials and also shows the importance of hydrostatic pressure in the yield condition for such materials. It should be noted that $f = 0$ implies that the material is fully dense and the Gurson yield condition reduces to that of Von Mises and $f = 1$ implies that the material is fully voided and has no stress carrying capacity. Compression of the material produces a strengthening effect due to closing of the voids, whereas because of opening of the voids in tension the material would soften.

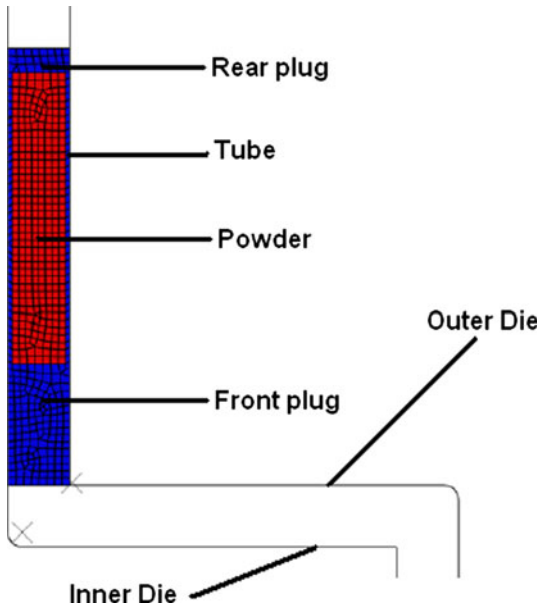

Fig. 1 The defined parts in the model

The two-dimensional finite element simulation for the ECAE was performed using finite element package ABAQUS/Explicit. Four parts were defined in the model, the inner part of the die, the outer part of the die, the powder, and the tube-plug as it is seen in Fig. 1. The inner and outer part of the die modeled using analytical rigid surface. For the copper tube and plugs a linear hardening elastic-plastic material model is used with Young's modulus of 110.3 GPa and initial yield stress of 80 MPa. For the powder the Gurson model was built into ABAQUS with an initial relative density of 0.9 (void volume fraction of 0.1). The interaction between the tube and the powder in the tangential direction was assumed frictionless because it seems rational that there is a relative motion between the tube and the powder. In the case of the interaction between the tube and the die, a friction value of 0.05 (Ref 39) was applied. An extrusion rate of 0.5 mm/s was used which is as the same as the experimental procedure. The double-pass ECAE was modeled in two steps. In the first step, the top surface is given a downward velocity which completes the first pass and in the second step, the left surface is given a horizontal velocity to the right to complete the second pass. This modeling is equivalent to rotating the work piece by 180° about its central axis (route C) (Ref 40) for the second pass. The two-dimensional simulations were carried out using plane strain condition. The powder, the tube, and the plugs were meshed using four node plane strain reduced elements (CPE4R) (Ref 34).

3. Experimental

Figure 2 shows the nitrogen gas atomized aluminum powder with mean particle diameter of 45 μm and an irregular shape which was used as the starting material. The compressibility of the powder was investigated by pressing the powder in a copper tube subjected to equal channel angular pressing. Aluminum powder in tubes (PITs) were prepared by closing one end of the tube with front plug and closing the other end by a rear plug

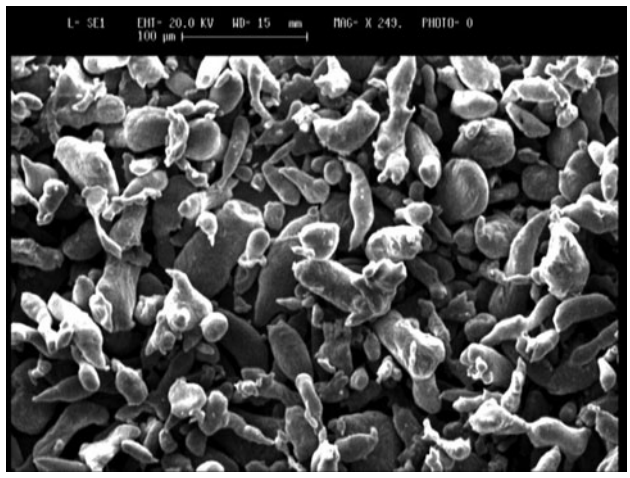

Fig. 2 SEM micrograph of nitrogen gas atomized aluminum powder with mean particle diameter of 45 μm and an irregular shape as the starting material

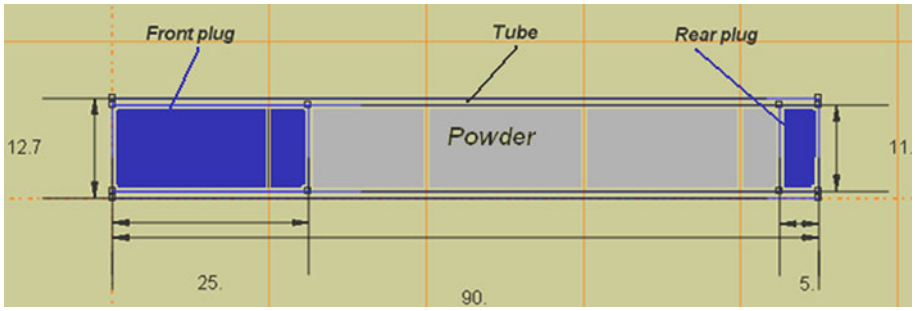

Fig. 3 Geometry and dimensions (in mm) of the tubes used

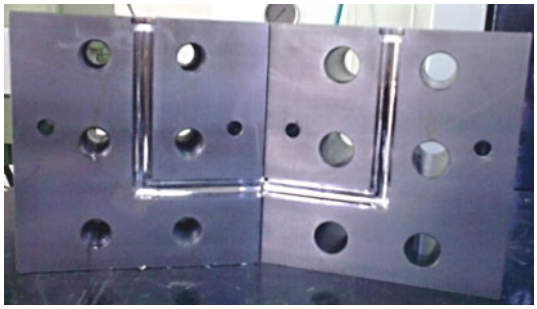

Fig. 4 ECAE split die used in this work

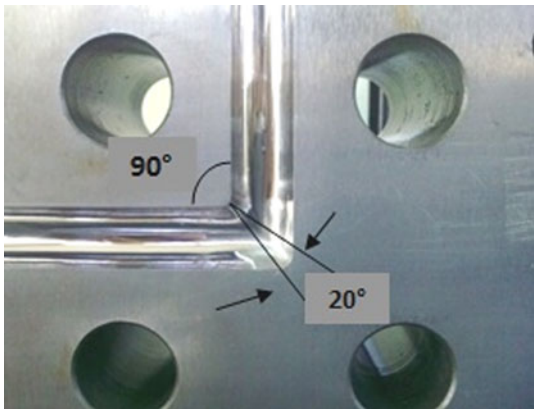

Fig. 5 Inner and outer angels of the die used in this work

after filling with the powder and compaction to a relative density of 90%. Front and rear plugs were prepared using copper. Geometry and dimensions (in mm) of the tubes used are shown in Fig. 3. These PITs were then subjected to multipass ECAE via route C, with a 20 ton press and the RAM speed of 0.5 mm/s at room temperature using ECAE split die (Fig. 4) with channel inner and outer angels of 90° and 20°(Fig. 5). Figure 6 shows the samples before, during and after one pass of ECAE. The density of the materials was measured based on the Archimedes principle using polished samples. Two lengths of front plug (25 and 45 mm) were used to investigate the effect of hydrostatic pressure on the amount of compressibility of the powders. Scanning electron microscopy and optical microscopy were performed on the longitudinal section to investigate the porosities during ECAE. For this purpose, first the surface of the sample was polished and then etched in a solution of

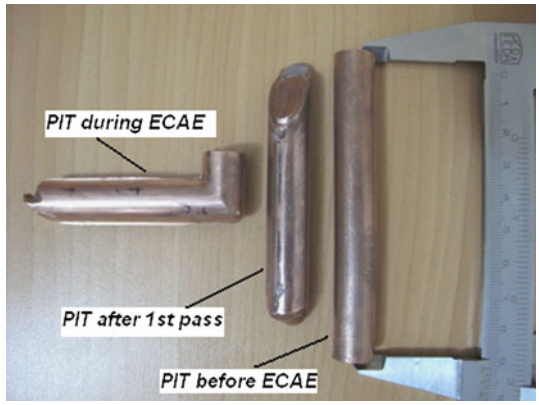

Fig. 6 Samples before, during, and after one pass of ECAE

15.5 mL HNO_3, 0.5 mL HF (48%), and 3.0 g CrO_3 in 84.0 mL H_2O (Graff/Surgent reagent). Hardness profile was taken from flow plane with a distance of 1 mm between indents. The Vickers hardness measurements (HV) were taken by applying a load of 1 kgf for 10 s.

4. Results and Discussion

From the void volume fraction contours after the first pass in Fig. 7(a), it is obvious that almost full densification is achieved near the inner corner and less near the outer corner of the intersecting channels after the first pass of ECAE, but as the densification proceeds in the second pass (Fig. 7b), the whole region consolidates uniformly. To further study the void volume fraction in the first pass of ECAE, three elements in the powder from inner edge, center, and the outer edge of the work piece are selected. For these elements, their void volume fraction and the hydrostatic pressure are tracked as they undergo the extrusion. Figure 8(a) and (b) show the sequence of shape evolution of the powder as it passes through the die by presenting three elements locating on the inner corner, center, and on the outer corner of the die in the first and in the second pass, respectively. From Fig. 9, which shows the void volume fraction with time period, one can see that the void volume fraction of the elements decreases continuously in region 1 due to front plug extrusion then it remains constant in region 2 until it passes through the corner completely (region 3). While the powder enters the exit channel (region 4), there is no change in the void volume fraction, until it goes through the second

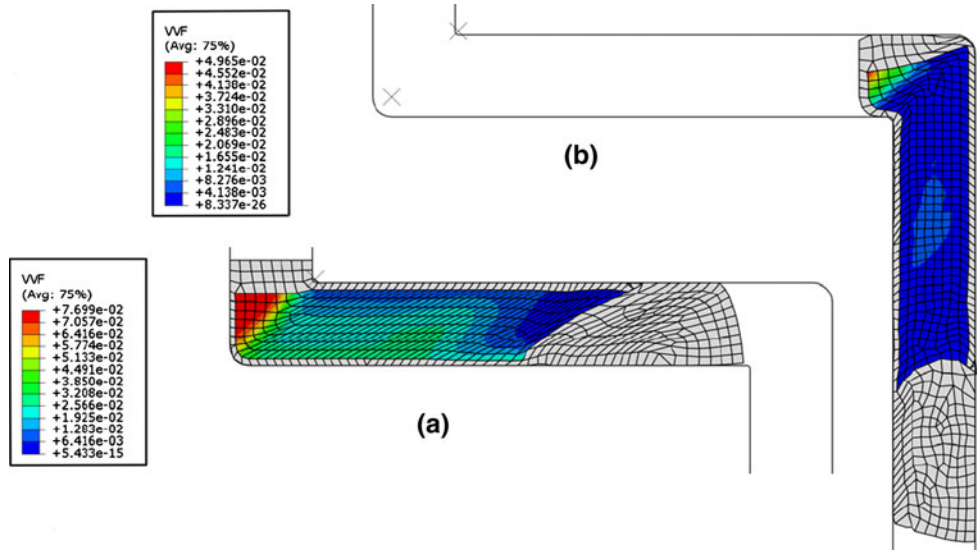

Fig. 7 Void volume fraction contours after (a) first pass and (b) second pass of ECAE

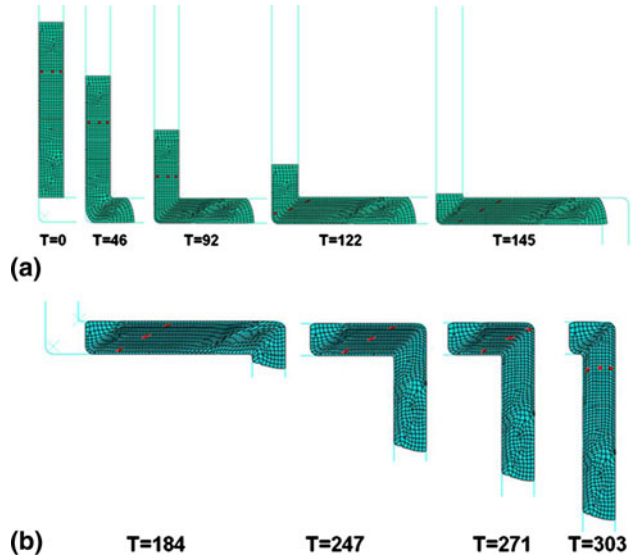

Fig. 8 The sequence of shape evolution of the powder as it passes through the die (a) in the first pass and (b) in the second pass

corner as the second pass of ECAE (region 5) in which further consolidation occurs and again there is no obvious decrease in void volume fraction of the elements as they enter the exit channel after the second pass (region 6).

It is obvious that the void volume fraction near the inner edge, center, and near the outer edge of the work piece, after the first pass is about 0.004, 0.012, and 0.020, respectively. The lower void volume fraction near the inner edge is mainly because of higher hydrostatic pressure which is experienced in the top portion than the bottom portion of the die. Figure 10 shows the hydrostatic pressure in the first pass of ECAE versus time period. It is seen that during the plug extrusion, the hydrostatic pressure reaches a maximum value of 225 MPa for three elements (inner edge, center, and outer edge). It means that during the extrusion of the front plug, similar hydrostatic pressure develops in these elements. After the extrusion of the whole length of the plug, the hydrostatic pressure decreases until the elements of the powder go through the die corner. The inner corner experiences higher hydrostatic pressure (248 MPa) than the outer corner (160 MPa) which is correspondent with the higher density near the inner edge than the outer edge.

In this article, we also investigated the effect of using a longer plug on the variation of void volume fraction after the first pass of ECAE. Figure 11 compares the void volume fractions after the first pass of ECAE for 45 and 25 mm plugs. Although there is no remarkable difference in the results between 25 and 45 mm plugs, during the front plug extrusion at $T = 31$, the void volume fraction is slightly lower in the powder with 45 mm plug (0.05) than with 25 mm plug (0.057).

To assure the finite element model, it should be validated by the experimental investigations. Optical microscopy after the first pass of ECAE from inner, center, and outer portion of the specimen in, respectively, validates the results. Figure 12(a)-(c) show more voids in the outer portion than the fully consolidated inner portion. Figure 12(d) also shows the elimination of pores near the outer portion of the work piece after the second pass of ECAE which confirms more uniform consolidation of powder especially near the outer portion after the second pass. Table 1 shows the relative density of the specimens after the first and the second pass of ECAE for both 25 and 45 mm plugs and compares them with the simulation results. It is seen that there is a good correlation between the simulations and the experiments. It is seen that an almost similar relative density is obtained by applying both 25 and 45 mm plugs. Note that the void volume fractions obtained from simulations have been changed to relative density for better comparison. It can be seen from the hardness profile in the flow plane of the compacted aluminum powder in Fig. 13(a) and (b) that there is a greater homogeneity in the inner portion of the specimen than the outer portion for both 25 and 45 mm plugs as can be seen from relatively low variation within the hardness profile near the inner edge. An abrupt decrease in the hardness profile may be due to two facts, first of all is the existence of the pores especially near the outer portion of the work piece. Second fact is the reduction of strain in the outer region of the strain hardening work piece due to corner gap in the edge region (Ref 41). Figure 14(a) and (b) depict pore distribution in the inner and outer edge of the work piece, respectively. It is seen that the pores are distributed homogonously in the matrix, so the reason for low hardness and also the

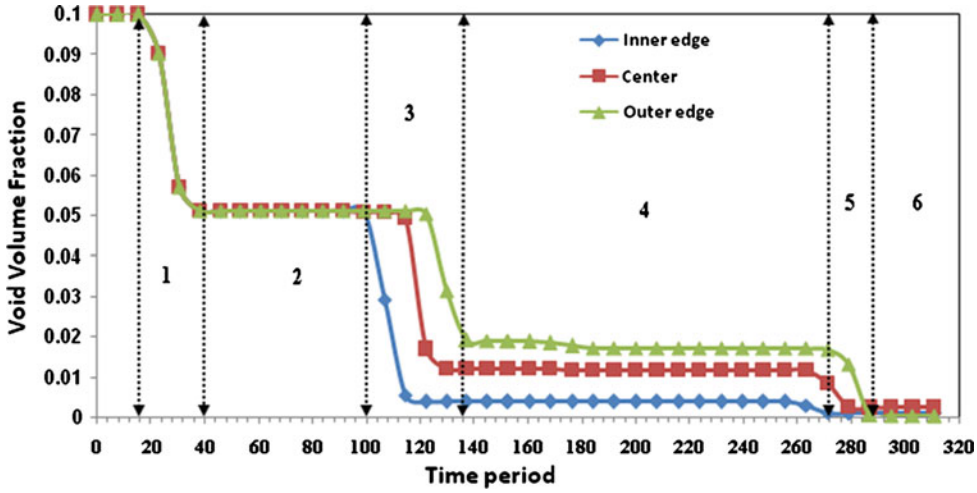

Fig. 9 The void volume fraction with time period for the first and second pass of ECAE

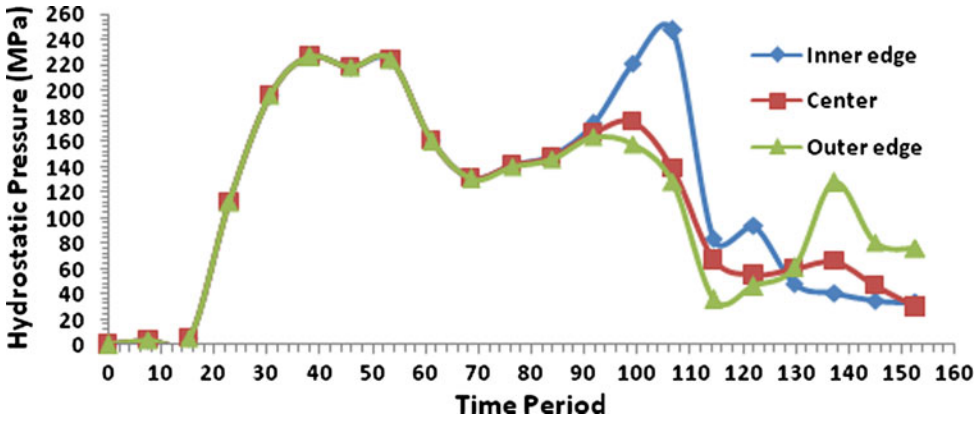

Fig. 10 The hydrostatic pressure during the first pass of ECAE vs. time period

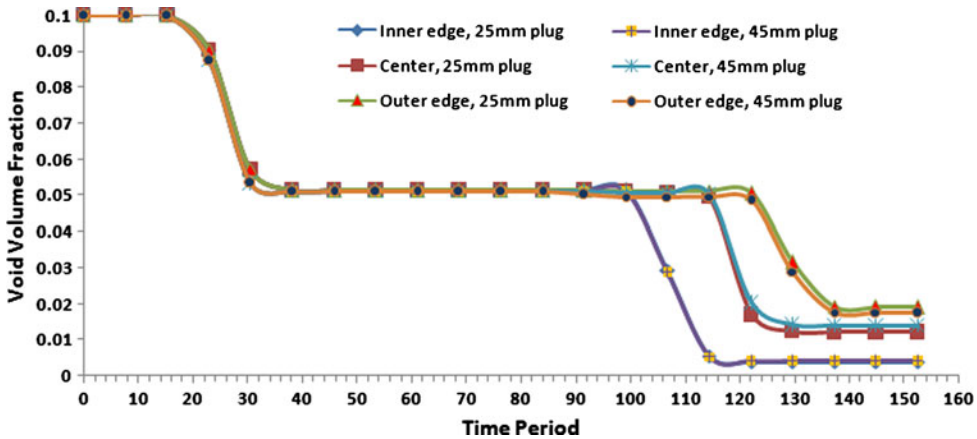

Fig. 11 A comparison between void volume fractions during the first pass of ECAE for 45 and 25 mm plugs

variation of the hardness in the outer edge can be attributed to low densification and low strain which the compacted powder experiences. Another point which is obtained from Fig. 13(a) and (b) is that the hardness increases gradually from outer edge to inner edge because of almost complete consolidation of powder near the inner edge. It is also visible in Fig. 13(c) that in the second pass the hardness increases particularly for the outer edge and a more uniform profile for inner portion, center, and outer portion of the specimen is obtained which presents consistent results with the simulations.

In this investigation, three rows of elements in the powder region were selected, and marked with section "A," section "B,"

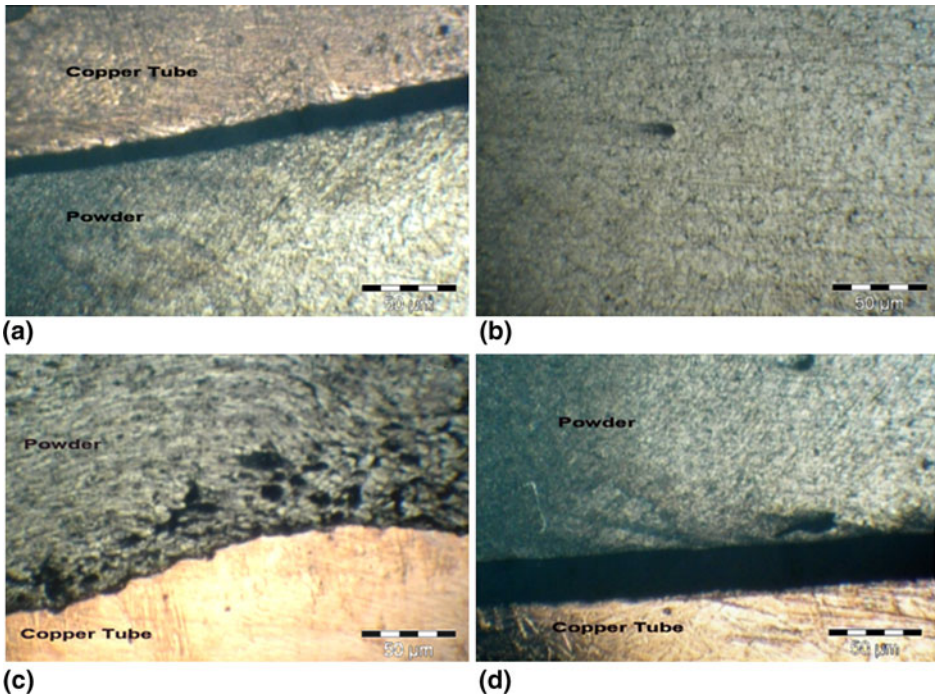

Fig. 12 Optical micrographs after the first pass of ECAE from (a) inner portion, (b) center, and (c) outer portion of the specimen. (d) After the second pass of ECAE from outer portion of the specimen

Table 1 Relative density of the specimens after the first and the second pass of ECAE for both 25 and 45 mm plugs

	Experimental	Simulation		
	Relative density, %	Relative density, %		
		Inner	Center	Outer
25 mm plug, first pass	97.19	99.61	98.79	97.91
25 mm plug, second pass	98.24	99.91	99.76	99.68
45 mm plug, first pass	97.43	99.72	98.61	98.12
45 mm plug, second pass	98.31	99.93	99.79	99.74

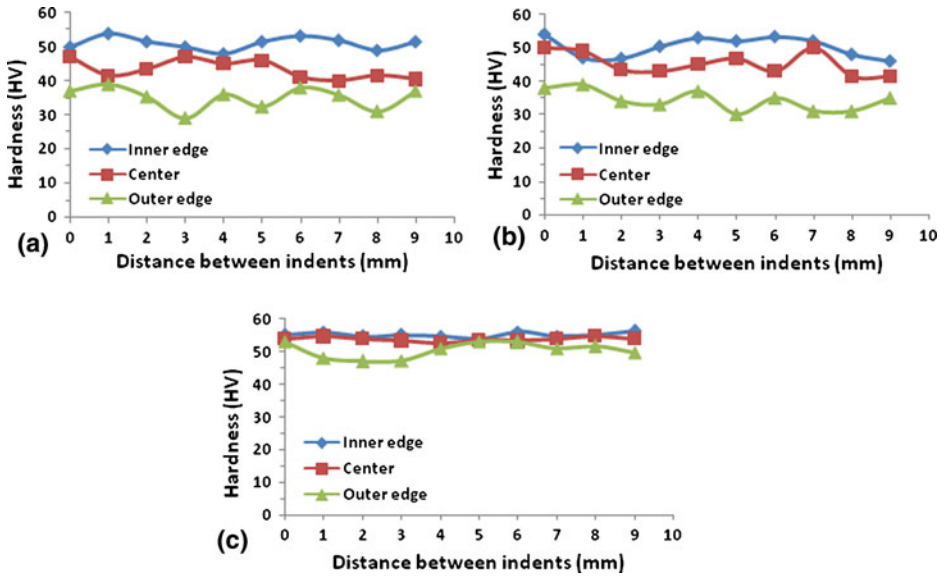

Fig. 13 The hardness profile in the flow plane of the compacted aluminum powder (a) after the first pass with 25 mm plug, (b) after the first pass with 45 mm plug, and (c) after the second pass with 25 mm plug

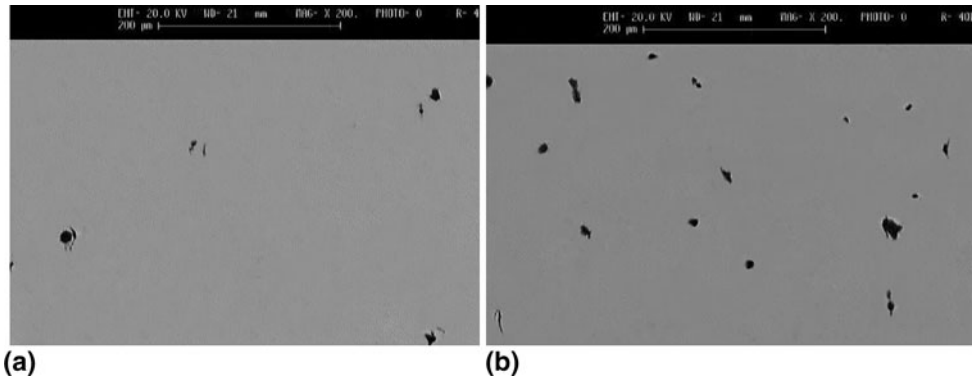

Fig. 14 SEM micrograph of the pore distribution after the first pass (a) in the inner edge and (b) outer edge of the work piece

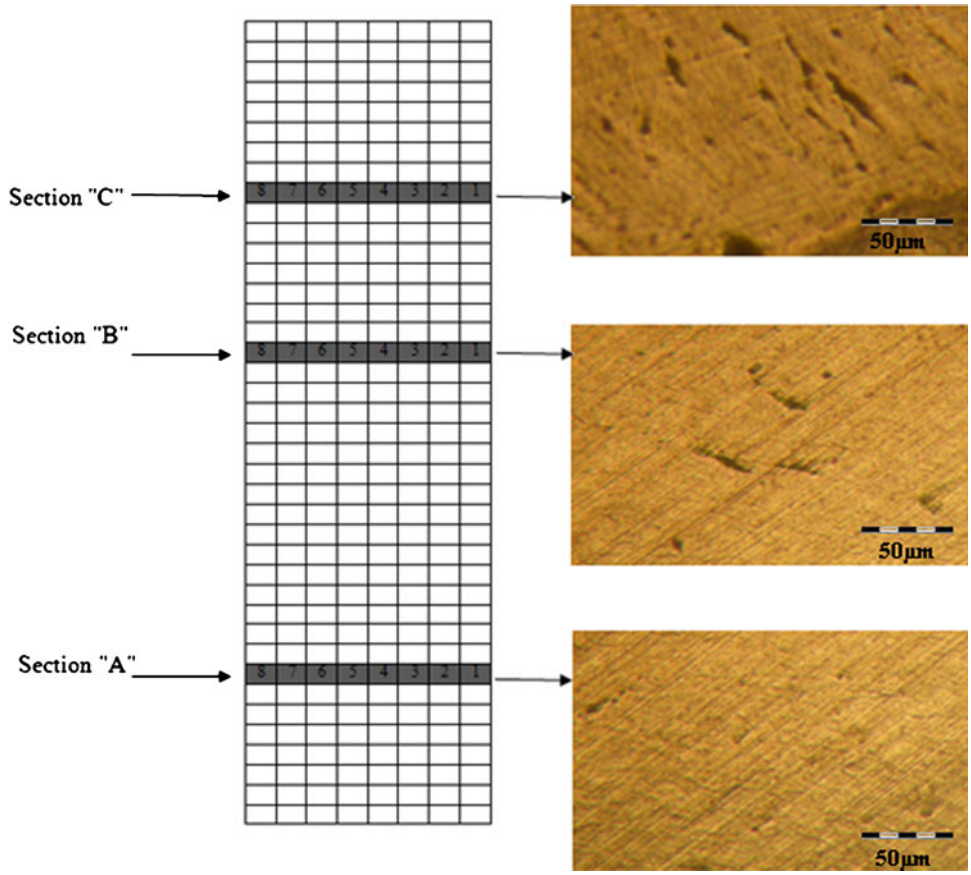

Fig. 15 The optical micrograph taken from the longitudinal plane from the center of the work piece near the leading end (section "A"), central portion (section "B"), and rear end (section "C")

and section "C" as are shown in Fig. 15. The optical micrographs of each section which are taken from the longitudinal plane from the center of the powder near the leading end (section "A"), central portion (section "B"), and rear end (section "C") are also obvious in this figure. The elements of the leading end at section "A" are consolidated better than the elements at section "C." One can also see the experimental results of the optical micrographs where the microvoids decrease gradually from the rear end to the leading end. In fact, this is due to higher hydrostatic pressure which the leading section experiences mainly because of its closer distance to the front plug.

Figure 16 also shows the void volume fraction against the element number in each section. As it is seen in this figure, the

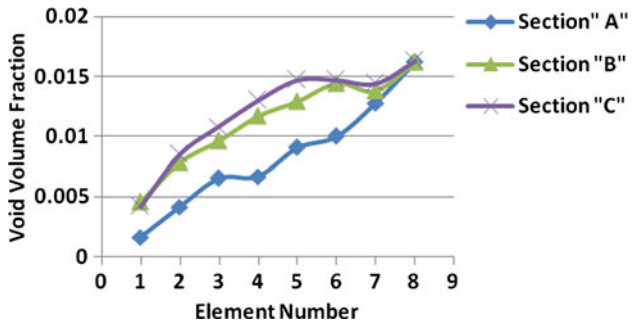

Fig. 16 Variation of void volume fraction against the element number in each section

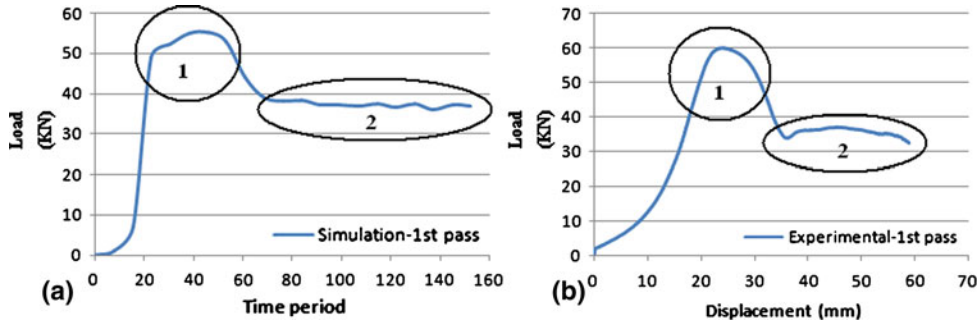

Fig. 17 The load-displacement curve for aluminum powder after the first pass of ECAE (a) simulated result and (b) experimental result

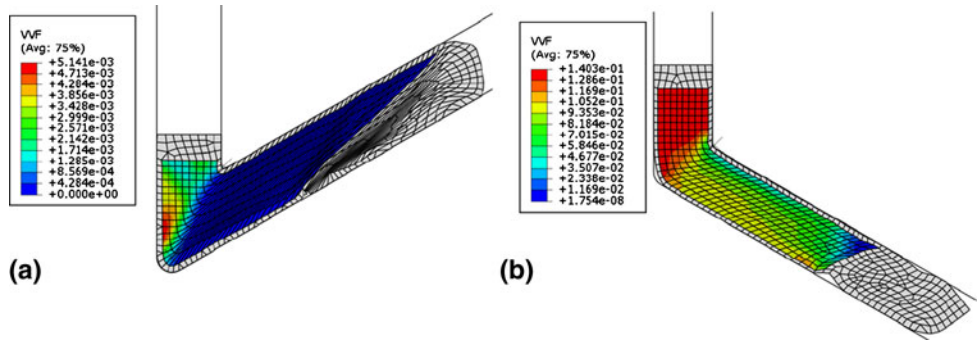

Fig. 18 The void volume fraction contour with 25 mm plug for (a) 60° angle die and (b) 120° angle die

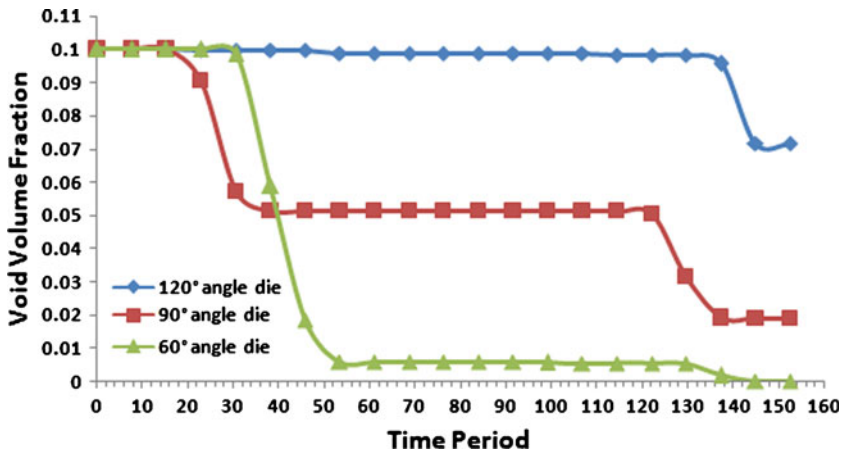

Fig. 19 Void volume fraction in 60°, 90°, and 120° angle die during the first pass of ECAE for the outer edge element

higher void volume fraction is achieved in section "C" and the void volume fraction increases from the inner element (1) to the outer element (8).

During powder consolidation via ECAE, the load-displacement curve was depicted. Figure 17(b) shows the experimental load-displacement curve for aluminum powder after the first pass of ECAE and Fig. 17(a) shows the load against time period during the ECAE simulation. As it is seen, the load increases gradually until it reaches a maximum point (region 1) and almost remains constant until the whole length of the front plug is extruded and then it decreases when the powder undergoes shear extrusion (region 2) and almost remains constant. The average load which is needed to apply shear on the powder as it is seen in Fig. 17(b) is about 38 kN which is almost comparable with the achieved load after the simulation in Fig. 17(a) where the specified regions on this figure are consistent with experimental load-displacement results.

After experimental validation of the simulations, our modeling was extended to consolidation of aluminum powder in a die with inner corner angle of 60° and 120° with the same outer angle of 20°. The same elements as in 90° angle die are selected to track the variation in void volume fraction and hydrostatic pressure. Figure 15 shows the void volume fraction contour for a 60° (Fig. 18a) and a 120° (Fig. 18b) angle die with 25 mm plug. As it is seen, in the 60° angle die the voids are eliminated and full density can be achieved after the first pass of ECAE which is consistent with Nagasekhar et al. (Ref 42) research. They showed that more than 80% of the

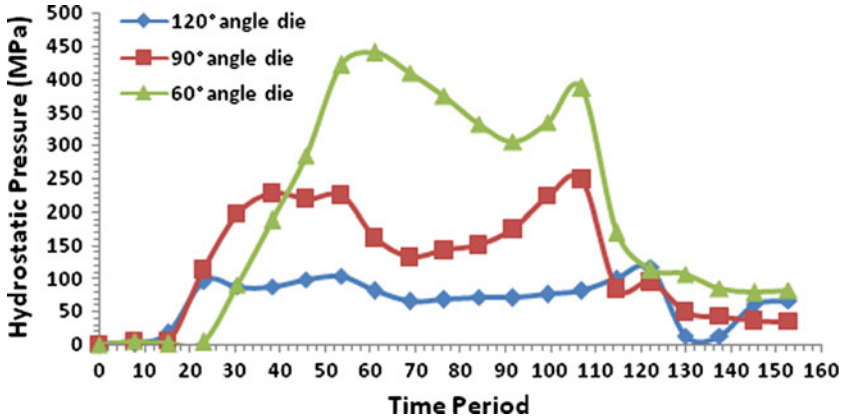

Fig. 20 Hydrostatic pressure in 60°, 90°, and 120° angle die during the first pass of ECAE for the inner edge element

cross section of the sample experiences uniform high strains in an acute channel angel. Whereas by applying lower level of strain in 120° angle die the material remains porous after the first pass of ECAE. Figure 19 shows the effectiveness of a sharper die angle in elimination of the residual porosities. Figure 20 compares the hydrostatic pressure in 60°, 90°, and 120° angle die after the first pass of ECAE for an inner edge element. The maximum hydrostatic pressure which is obtained during the front plug extrusion in 60° angle die is about 440 MPa and is about two times greater than the maximum hydrostatic pressure which is obtained in 90° angle die (225 MPa), but the hydrostatic pressure is really low in 120° angle die (103 MPa) which confirms the high void volume fraction in 120° angle die.

5. Conclusions

In this work, the process of powder compaction through ECAE was simulated using finite element package ABAQUS. The Gurson model was implemented. In the 2-D simulations, the powder was modeled in a copper tube with front and rear plugs in a 90° angle die. The powder near the inner edge consolidates almost completely whereas the powder at the outer edge does not. This is mainly because of higher hydrostatic pressure which is developed near the inner edge. The void volume fraction decreases from 0.1 to about 0.05 during the front plug extrusion and remains constant until the powder reaches the bend, where the majority of the voids are eliminated and the void volume fraction reaches to about 0.004 to 0.02 after the first pass of ECAE depending on the location of the element. During the second pass, full and uniform densification is obtained. It can be seen through the simulations that application of longer front plug (45 mm) in developing higher hydrostatic pressure (more than 225 MPa) is negligible and the final relative density is the same as applying a 25 mm plug. The simulations were also carried out for 60° and 120° angle die. It is observed that complete and uniform densification is achieved after the first pass in a 60° angle die, but the material is still porous after one pass of ECAE in a 120° angle die because of lower hydrostatic pressure which is developed in a 120° angle die. Future work using the simulation developed in this work can include carrying out a study to optimize the process variables like friction between the walls of the die and the tube, the rate of extrusion, tube material, and number of passes. The process can also be extended to 3-D simulations in the future works.

References

1. V.M. Segal, Materials Processing by Simple Shear, *Mater. Sci. Eng. A*, 1995, **197**, p 157–164
2. Y. Iwahashi, Z. Horita, M. Nemoto, and T.G. Langdon, An Investigation of Microstructural Evolution During Equal-Channel Angular Pressing, *Acta Mater.*, 1997, **45**, p 4733–4741
3. Y. Iwahashi, Z. Horita, M. Nemoto, and T.G. Langdon, Factors Influencing the Equilibrium Grain Size in Equal-Channel Angular Pressing: Role of Mg Additions to Aluminum, *Metall. Mater. Trans. A*, 1998, **29**, p 2503–2512
4. R.Z. Valiev, R.K. Islamgaliev, and I.V. Alexandrov, Bulk Nanostructured Materials From Severe Plastic Deformation, *Prog. Mater. Sci.*, 2000, **45**, p 103–110
5. V.M. Segal, Equal Channel Angular Extrusion: From Macromechanics to Structure Formation, *Mater. Sci. Eng. A*, 1999, **271**, p 322–333
6. V.M. Segal, Engineering and Commercialization of Equal Channel Angular Extrusion (ECAE), *Mater. Sci. Eng. A*, 2004, **386**, p 269–276
7. Y.T. Zhu and T.C. Lowe, Observations and Issues on Mechanisms of Grain Refinement During ECAP Process, *Mater. Sci. Eng. A*, 2000, **291**, p 46–53
8. R. Srinivasan, Computer Simulation of the Equal Channel Angular Extrusion (ECAE) Process, *Scr. Mater.*, 2001, **44**, p 91–96
9. T. Suo, Y. Li, Y. Guo, and Y. Liu, The Simulation of Deformation Distribution During ECAP Using 3D Finite Element Method, *Mater. Sci. Eng. A*, 2006, **432**, p 269–274
10. I. Balasundar, M. Sudhakara Rao, and T. Raghu, Equal Channel Angular Pressing Die to Extrude a Variety of Materials, *Mater. Des.*, 2009, **30**, p 1050–1059
11. S. Xu, G. Zhao, G. Ren, and X. Ma, Numerical Simulation and Experimental Investigation of Pure Copper Deformation Behavior for Equal Channel Angular Pressing/Extrusion Process, *Comput. Mater. Sci.*, 2008, **44**, p 247–252
12. A.V. Nagasekhar and Y. Tick-Hon, Optimal Tool Angles for Equal Channel Angular Extrusion of Strain Hardening Materials by Finite Element Analysis, *Comput. Mater. Sci.*, 2004, **30**, p 489–495
13. P. Leo, E. Cerri, P.P. De Marco, and H.J. Roven, Properties and Deformation Behaviour of Severe Plastic Deformed Aluminum Alloys, *J. Mater. Process. Technol.*, 2007, **182**, p 207–214
14. A.V. Nagasekhar, Y. Tick-Hon, and H.P. Seow, Deformation Behavior and Strain Homogeneity in Equal Channel Angular Extrusion/Pressing, *J. Mater. Process. Technol.*, 2007, **192–193**, p 449–452
15. B.S. Moon, H.S. Kim, and S.I. Hong, Plastic Flow and Deformation Homogeneity of 6061 Al During Equal Channel Angular Pressing, *Scr. Mater.*, 2002, **46**, p 131–136

16. C.J. Luis Perez, P. Gonzales, and Y. Garces, Channel Angular Extrusion in a Commercial Al-Mn Alloy, *J. Mater. Process. Technol.*, 2003, **143–144**, p 506–511
17. G.M. Stoica, D.E. Fielden, R. McDaniels, Y. Liu, B. Huang, P.K. Liaw, C. Xu, and T.G. Langdon, An Analysis of the Shear Zone for Metals Deformed by Equal-Channel Angular Processing, *Mater. Sci. Eng. A*, 2005, **410–411**, p 239–242
18. S. Li, M.A.M. Bourke, I.J. Beyerlein, D.J. Alexander, and B. Clausen, Finite Element Analysis of the Plastic Deformation Zone and Working Load in Equal Channel Angular Extrusion, *Mater. Sci. Eng. A*, 2004, **382**, p 217–236
19. J.Y. Suh, H.S. Kim, J.W. Park, and J.Y. Chang, Finite Element Analysis of Material Flow in Equal Channel Angular Pressing, *Scr. Mater.*, 2001, **44**, p 677–681
20. S.J. Oh and S.B. Kang, Analysis of the Billet Deformation During Equal Channel Angular Pressing, *Mater. Sci. Eng. A*, 2003, **343**, p 107–115
21. S.W. Chung, H. Somekawa, T. Kinoshita, W.J. Kim, and K. Higashi, The Non-Uniform Behavior During ECAE Process by 3-D FVM Simulation, *Scr. Mater.*, 2004, **50**, p 1079–1083
22. O.N. Senkov, S.V. Senkova, J.M. Scott, and D.B. Miracle, Compaction of Amorphous Aluminum Alloy Powder by Direct Extrusion and Equal Channel Angular Extrusion, *Mater. Sci. Eng. A*, 2005, **393**, p 12–21
23. A.V. Nagasekhar, Y. Tick-Hon, R.K. Guduru, and K.S. Ramakanth, Multipass Equal Channel Angular Extrusion of MgB_2 Powder in Tubes, *Physica C*, 2007, **466**, p 174–180
24. P. Quang, Y.G. Jeong, S.H. Hong, and H.S. Kim, Equal Channel Angular Pressing of Carbon Nanotube Reinforced Metal Matrix Nanocomposites, *Key. Eng. Mater.*, 2006, **326–328**, p 325–328
25. I. Karaman, M. Haouaoui, and H.J. Maier, Nanoparticle Consolidation Using Equal Channel Angular Extrusion at Room Temperature, *J. Mater. Sci.*, 2007, **42**, p 1561–1576
26. K. Matsuki, T. Aida, T. Takeuchi, J. Kusui, and K. Yokoe, Microstructural Characteristics and Superplastic-Like Behavior in Aluminum Powder Alloy Consolidated by Equal-Channel Angular, *Acta Mater.*, 2000, **48**, p 2625–2632
27. J. Robertson, J.T. Im, I. Karaman, K.T. Hartwig, and I.E. Anderson, Consolidation of Amorphous Copper Based Powder by Equal Channel Angular Extrusion, *J. Non-Cryst. Solids*, 2003, **317**, p 144–151
28. A.T. Procopioa and A. Zavaliangos, Simulation of Multi-Axial Compaction of Granular Media from Loose to High Relative Densities, *J. Mech. Phys. Solids*, 2005, **53**, p 1523–1551
29. W. Wu, G. Jiang, R.H. Wagoner, and G.S. Daehn, Experimental and Numerical Investigation of Idealized Consolidation Part 1: Static Compaction, *Acta Mater.*, 2000, **48**, p 4323–4330
30. L.H. Han, J.A. Elliott, A.C. Bentham, A. Mills, G.E. Amidon, and B.C. Hancock, A Modified Drucker-Prager Cap Model for Die Compaction Simulation of Pharmaceutical Powders, *Int. J. Solid. Struct.*, 2008, **45**, p 3088–3106
31. H.S. Kim, M.H. Seo, C.-S. Oh, and S.-J. Kim, Equal Channel Angular Pressing of Metallic Powders, *Mater. Sci. Forum*, 2003, **437–438**, p 89–92
32. S.C. Yoon and H.S. Kim, Equal Channel Angular Pressing of Metallic Powders for Nanostructured Materials, *Mater. Sci. Forum*, 2006, **503–504**, p 221–226
33. S.C. Yoon, S.-J. Hong, S.I. Hong, and H.S. Kim, Mechanical Properties of Equal Channel Angular Pressed Powder Extrudates of Rapidly Solidified Hypereutectic Al-20 wt% Si Alloy, *Mater. Sci. Eng. A*, 2007, **449–451**, p 966–970
34. S.C. Lee, S.Y. Ha, K.T. Kim, S.M. Hwang, L.M. Huh, and H.S. Chung, Finite Element Analysis for Deformation Behavior of an Aluminum Alloy Composite Containing SiC Particles and Porosities During ECAP, *Mater. Sci. Eng. A*, 2004, **371**, p 306–312
35. A.L. Gurson, Continuum Theory of Ductile Rupture by Void Nucleation and Growth: Part I—Yield Criteria and Flow Rules for Porous Ductile Materials, *J. Eng. Mater. Technol.*, 1977, **99**, p 2–15
36. Abaqus Inc, *Abaqus Users Manual*, Version 6.8-1, 2008
37. D.P. Delo and R.H. Piehler, Early Stage Consolidation Mechanisms During Hot Isostatic Pressing of Ti-6Al-4V Powder Compacts, *Acta Mater.*, 1999, **47**, p 2841–2852
38. K.T. Kim and M.M. Carroll, Compaction Equations for Strain Hardening Porous Materials, *Int. J. Plast.*, 1987, **3**, p 63–73
39. A.V. Nagasekhar, S.C. Yoon, Y. Tick-Hon, and H.S. Kim, An Experimental Verification of the Finite Element Modelling of Equal Channel Angular Pressing, *Comput. Mater. Sci.*, 2009, **46**, p 347–351
40. M. Furukawa, Z. Horita, and T.G. Langdon, Processing by Equal Channel Angular Pressing: Applications to Grain Boundary Engineering, *J. Mater. Sci.*, 2005, **40**, p 909–917
41. H.S. Kim, M.H. Seo, and S.I. Hong, On the Die Corner Gap Formation in Equal Channel Angular Pressing, *Mater. Sci. Eng. A*, 2000, **291**, p 86–90
42. A.V. Nagasekhar, Y. Tick-Hon, S. Li, and H.P. Seow, Effect of Acute Tool Angles on Equal Channel Angular Extrusion/Pressing, *Mater. Sci. Eng. A*, 2005, **410–411**, p 269–272